

Highly ordered palladium nanodots and nanowires from switchable block copolymer thin films

This article has been downloaded from IOPscience. Please scroll down to see the full text article.

2009 Nanotechnology 20 415302

(<http://iopscience.iop.org/0957-4484/20/41/415302>)

View [the table of contents for this issue](#), or go to the [journal homepage](#) for more

Download details:

IP Address: 165.91.74.118

The article was downloaded on 07/07/2013 at 19:57

Please note that [terms and conditions apply](#).

Highly ordered palladium nanodots and nanowires from switchable block copolymer thin films

E Bhoje Gowd^{1,4}, Bhanu Nandan^{1,4}, Mukesh Kumar Vyas¹,
Nadja C Bigall², Alexander Eychmüller², Heike Schlörb³
and Manfred Stamm¹

¹ Leibniz Institute of Polymer Research Dresden, Hohe Strasse 6, 01069, Dresden, Germany

² Physical Chemistry and Electrochemistry, TU Dresden, Bergstrasse 66b, 01062, Dresden, Germany

³ Leibniz Institute for Solid State and Materials Research Dresden, PO Box 27 00 16, D-01171, Dresden, Germany

E-mail: gowd@ipfdd.de and nandan@ipfdd.de

Received 20 July 2009, in final form 27 August 2009

Published 18 September 2009

Online at stacks.iop.org/Nano/20/415302

Abstract

We demonstrate a new approach to fabricate highly ordered arrays of nanoscopic palladium dots and wires using switchable block copolymer thin films. The surface-reconstructed block copolymer templates were directly deposited with palladium nanoparticles from a simple aqueous solution. The preferential interaction of the nanoparticles with one of the blocks is mainly responsible for the lateral arrangement of the nanoparticles inside the pores of the templates in addition to the capillary forces. A subsequent stabilization by UV-irradiation followed by pyrolysis in air at 450 °C removes the polymer to produce highly ordered metallic nanostructures. We extended this approach to micellar films to obtain metallic nanostructures. This method is highly versatile as the procedure used here is simple, eco-friendly and provides a simple approach to fabricate a broad range of nanoscaled architectures with tunable lateral spacing, and can be extended to systems with even smaller dimensions.

 Supplementary data are available from stacks.iop.org/Nano/20/415302

(Some figures in this article are in colour only in the electronic version)

1. Introduction

Nanofabrication, the generation of ultrafine structures, is central to modern technology and the key for producing many revolutionary structures with applications such as powerful electronic/optical devices, miniaturized sensors, human biomedical replacements and other advanced technological devices [1–4]. In general, a feature size greater than 500 nm is routinely produced by photolithography techniques, and for sizes between 500 and 30 nm, electron beam lithography is commonly used. However, a feature size less than 30 nm is hard to achieve with the above-mentioned standard semiconductor lithography techniques. Industry is

still searching for alternative patterning approaches in order to tackle the challenge of feature sizes less than 30 nm. The construction of nanostructures via the self-assembly of molecular-sized components, the so-called ‘bottom-up’ chemical approach is the method of choice to effect this goal, as this method offers a number of potentially attractive advantages. Recently, block copolymer self-assembling systems have attracted immense interest for nanofabrication because they spontaneously generate highly ordered structures with nanometer precision, and they are simple and cost-effective processes for fabrication [5, 6]. The compatibility of these systems with the existing silicon-based technology makes them even more attractive.

Block copolymers are exemplary self-assembling systems which, in thin films, have shown great potential as

⁴ Authors to whom any correspondence should be addressed.

templates [7–11]. These materials tend to form ordered, periodic microdomains including spheres, cylinders, and lamellae with typical dimensions of 5–50 nm [12–15]. The size and shape of the microdomains can be controlled by manipulating the chain lengths, the chemical functionality, the volume fraction of each block, and the temperature. Controlling the orientation and lateral ordering of the microdomain is one of the important issues in thin films and various strategies have been developed for inducing a large area orientation of block copolymer microdomain patterns [10, 16, 17]. Among these nanostructures, block copolymers with cylindrical microdomains are of particular interest because elimination of the minor component or surface reconstruction in a selective solvent transforms the structures into nanopore arrays [10, 18–20]. Block copolymer templates thus obtained were exploited to achieve secondary patterns of interest by several methods including chemical and physical vapor deposition, electrodeposition, incorporation of metal nanoparticles and chemical reduction techniques [9, 10, 18, 21–24].

The organization of inorganic nanoparticles within self-assembled templates has attracted the attention of scientists, as this process is simple, versatile and does not need external fields for depositing nanoparticles into the block copolymer domains [9, 21–40]. A number of methods have been developed to selectively incorporate metallic nanoparticles into the desired block copolymer domains. In one method, pre-synthesized metallic nanoparticles of desired size, shape and surface chemistry are mixed with block copolymer to produce nanopatterned block copolymer-supported arrays [26, 27]. In this method the metallic nanoparticles have been modified in such a way that they selectively favor solubilization in one block of the polymer. Balazs and co-workers have recently suggested that the position of the nanoparticles can be controlled by adjusting the size of the nanoparticle and the size of the block copolymer domain [28, 29]. In another method, the nanoparticles are synthesized *in situ* within the block copolymer template by using preformed micelles of block copolymer containing metal precursors [23, 30–35]. Buriak and co-workers have recently used block copolymer templates to form nanoparticle arrays on semiconducting surfaces [36, 37]. Their approach involves selective loading of metal ions on to the acid responded block copolymer domain followed by an oxygen plasma treatment to reduce the metal ions to metallic nanostructures. Lo *et al* [23] used a pore-filling process for the fabrication of semiconductor nanoarrays from PS nanoporous templates, which involved the thrust of capillary force driven from the tunable wetting property of the templates. All these methods for the metal patterning with their various mechanisms were involved in the dispersion process of the nanoparticles within the polymer film and make it difficult to understand the kinetics of nanoparticle formation in the polymer matrix. Very little focus has been made on the direct deposition of pre-synthesized nanoparticles onto pre-patterned block copolymer nanotemplates. For example, Russell and co-workers have utilized polystyrene-*block*-poly(methyl methacrylate) (PS-*b*-PMMA) block copolymer thin films, whereby the minority

component PMMA was removed by UV photodegradation to form a nanoporous template [41]. In one method, capillary forces were used to drive CdSe nanoparticles into the nanopores of cylindrical diblock copolymer templates [21]. In another one, electrophoretic deposition was used to drive these nanoparticles into the nanopores and nanotrenches of diblock copolymer templates [22]. In these methods, the lateral distribution of the nanoparticles into the nanopores was purely manipulated by physical forces such as capillary forces or electric fields. The direct deposition process, however, offers a better method if one can manipulate the distribution of the nanoparticles in the nanopores by chemical methods, in addition to physical methods, in order to obtain uniform structures. Therefore, one of the polymer blocks chosen should have a specific function, e.g. coordination capabilities to the surface of the nanoparticles.

In this work, a new approach to fabricate highly ordered arrays of palladium nanodots and nanowires is demonstrated using switchable block copolymer thin films. For that purpose, surface-reconstructed thin films of polystyrene-*b*-poly(4-vinylpyridine) (PS-*b*-P4VP) having different morphologies were used as templates. This block copolymer was chosen because it contains reactive pyridine groups, which can selectively bind to the metal nanoparticles surfaces and also because it can form hydrophilic nanopores, which can be easily wetted with aqueous solution. In addition, pronounced repulsive interactions between PS and P4VP allowed the fabrication of nanopatterns with sub-30 nm periodicity. Deposition of pre-synthesized nanoparticles into the templates, followed by removal of the polymer, led to highly ordered metallic patterns identical to the order of the parent template. This technique allows the production of arrays of metallic nanoparticles on silica surfaces with precise control over particle size and interparticle spacing. We also extended this approach to PS-*b*-P4VP micellar films to obtain the complementary structures in nanoscale.

2. Experimental details

Synthesis of nanoparticles. Palladium(II) chloride with 99.999% purity was purchased from Sigma-Aldrich. Palladium(II) chloride was dissolved in concentrated hydrochloric acid in the ratio PdCl₂:HCl 1:2, followed by dilution with deionized water, so that the final precursor concentration was 10 mM. The solution was filtered using a hydrophilic syringe filter with a 0.2 μm pore size. 88.5 ml of deionized water (MilliQ) was heated to 80 °C in a round flask under a reflux condenser. 2.5 ml of the precursor were added, followed 1 min later by the addition of 2 ml of a 1% sodium citrate solution. To 50 ml of a 1% sodium citrate solution 0.038 ml sodium borohydride were added, and 1 ml of the resulting solution was quickly injected to the reaction mixture (1 min after the addition of the citrate solution). After 10 min the brown solution was cooled down to room temperature. The resulting nanoparticle solution was filtered using a syringe filter (0.2 μm pore size).

Fabrication of nanotemplates and nanoparticle deposition. Two kinds of PS-*b*-P4VP with different M_n were purchased

from Polymer Source, Inc. and used without further purification. PS-*b*-P4VP with $M_n = 40.9 \text{ kg mol}^{-1}$ ($M_n^{\text{PS}} = 32.9 \text{ kg mol}^{-1}$; $M_n^{\text{P4VP}} = 8.0 \text{ kg mol}^{-1}$) and polydispersity of 1.06 was dissolved in chloroform to obtain a 1 wt% polymer solution. The polymer solutions were filtered several times through Millipore 0.2 μm Teflon filters. Thin films were prepared by a dip-coating process at a speed of 1.0 mm s^{-1} onto the silicon wafers, which were cleaned with dichloromethane in an ultrasonic bath for 20 min followed by further cleaning in a 1:1:1 mixture of 29% ammonium hydroxide, 30% hydrogen peroxide and water (*Warning: this solution is extremely corrosive and should not be stored in tightly sealed containers*) for 1.5 h at 65°C . These single-crystal silicon wafers of {100} orientation were purchased from Semiconductor Processing Co. The films were exposed to different solvent vapors in a sealed glass chamber to obtain the desired cylindrical orientation. The chamber was opened to allow the solvent to evaporate freely once an approximate swelling ratio 2.75 was reached in the BC thin film. Finally, these thin films were immersed in ethanol for 20 min to prepare nanoporous structures. These nanoporous templates were dipped in an aqueous solution of nanoparticles for 1 h. After removal, templates were repeatedly washed with deionized water in order to ensure the complete removal of the non-adsorbed or weakly adsorbed nanoparticles. The nanoparticle deposited templates were then cross-linked using a 254 nm germicidal UV lamp (type G8T5, 2.5 W, TecWest, Inc., USA). The polymer was removed by pyrolysis in an air furnace at 450°C for 2 h. Separately, PS-*b*-P4VP copolymer (molecular weight of 39.0 kg mol^{-1} ($M_n^{\text{PS}} = 20.0 \text{ kg mol}^{-1}$; $M_n^{\text{P4VP}} = 19.0 \text{ kg mol}^{-1}$) and polydispersity of 1.09) was dissolved in toluene/THF (80/20 v/v) solvent mixture at 70°C for 2 h to yield a 1 wt% polymer solution. In this, the micelles were coated on the silicon substrate by dip-coating as mentioned above. These micelles were further annealed in toluene/THF (80/20 v/v) vapors for 8 h to improve the long-range order and further annealing in 1,4-dioxane vapors resulted in perpendicular lamellae. Metallic nanostructures were obtained using the same procedure as discussed above. In this case, samples were annealed in ethanol vapors for 20 min to reconstruct the surface instead of immersing the sample directly in ethanol. Scanning force microscopy (Digital Instruments, Inc., Santa Barbara) (SFM) imaging was performed using a Dimension 3100 and a CP microscope (Park Scientific Instrument, Inc.) in the tapping mode. High-resolution scanning electron microscopy (HRSEM) was performed using a Zeiss Ultra 55 Gemini scanning electron microscope with an acceleration voltage of 5 kV. The film thickness was measured by ellipsometry (SENTECH Instruments GmbH, Germany). XPS experiments were performed with an AXISULTRA spectrometer (Kratos Analytical, UK) equipped with a monochromatized Al K α x-ray source of 300 W at 20 mA.

3. Results and discussion

Figure 1 illustrates the fabrication of palladium nanodots and nanowires using a block copolymer thin film. Dip-coated

samples, which are in a disordered state, were further annealed in saturated vapors of an appropriate solvent to improve the long-range order. The orientation of the cylindrical microdomains is found to change with the vapors of an appropriate solvent. For example, annealing in 1,4-dioxane results in cylindrical microdomains normal to the surface (figure 1(a)), while a mixture of toluene/THF (80/20 v/v) leads to cylindrical microdomains parallel to the surface (figure 1(b)). Furthermore, the orientation of the cylindrical microdomains reversibly switches upon annealing in vapors of an appropriate solvent. Dipping these ordered thin films in ethanol, which is a selective solvent for P4VP, results in the formation of nanoporous templates (figures 1(c) and (d)). By immersing the nanotemplates in aqueous solutions of nanoparticles, the hydrophilic P4VP chains, which are on the walls of the nanopores, wet thoroughly and preferentially attract the nanoparticles, while the hydrophobic PS matrix remains unaltered (figures 1(e) and (f)). The resulting hybrid thin films are stabilized under UV-irradiation, and subsequent pyrolysis at 450°C removes the cross-linked block copolymer films completely leaving well-defined metallic nanodots (figure 1(g)) and nanowires (figure 1(h)) on the silicon substrate.

Block copolymer thin films were prepared by a dip-coating process using 1 wt% PS-*b*-P4VP ($M_n^{\text{PS}} = 32.9 \text{ kg mol}^{-1}$; $M_n^{\text{P4VP}} = 8.0 \text{ kg mol}^{-1}$) chloroform solutions onto silicon wafers. Figure 2 shows the scanning force microscopy (SFM) height images of the samples as dip-coated, solvent annealed in 1,4-dioxane and toluene/THF (80/20 v/v) solvent mixtures, and the corresponding structures after the surface reconstruction. The SFM images of an as dip-coated film (figure 2(a)) showed a disordered wormlike pattern due to fast solvent evaporation, leaving the chains insufficient time to rearrange to attain equilibrium morphology. 1,4-dioxane vapor annealed thin films assemble into hexagonally packed cylindrical microdomains oriented normal to the substrate ($C\perp$) (figure 2(b)). On the other hand, the samples annealed in a mixture of toluene/THF (80/20) showed well-developed cylindrical microdomains parallel to the substrate ($C\parallel$) (figure 2(c)). Chloroform and dimethylformamide can also be used to orient the cylinders parallel to the substrate ($C\parallel$). Furthermore, we have found that the orientation of the cylindrical domains switches upon annealing in vapors of an appropriate solvent. For example, annealing the thin film with $C\perp$ cylindrical domains (figure 2(b)) in saturated vapors of toluene/THF mixture leads to the re-orientation of microdomains to $C\parallel$ (figure 2(c)). Opposite to this, annealing the films with $C\parallel$ cylindrical microdomains (figure 2(c)) in saturated 1,4-dioxane vapors results in switching the orientation to hexagonally packed $C\perp$ cylindrical microdomains (figure 2(b)). The re-orientation of cylinders is relatively fast, and can be repeated several times. The solvent evaporation and the selectivity of the solvent to constituted blocks may be mainly responsible for the switching behavior in block copolymer thin films. The mechanism of switching in PS-*b*-P4VP diblock copolymer thin films is not yet fully understood. Sidorenko *et al* [42, 43] demonstrated such switching phenomena in a supramolecular

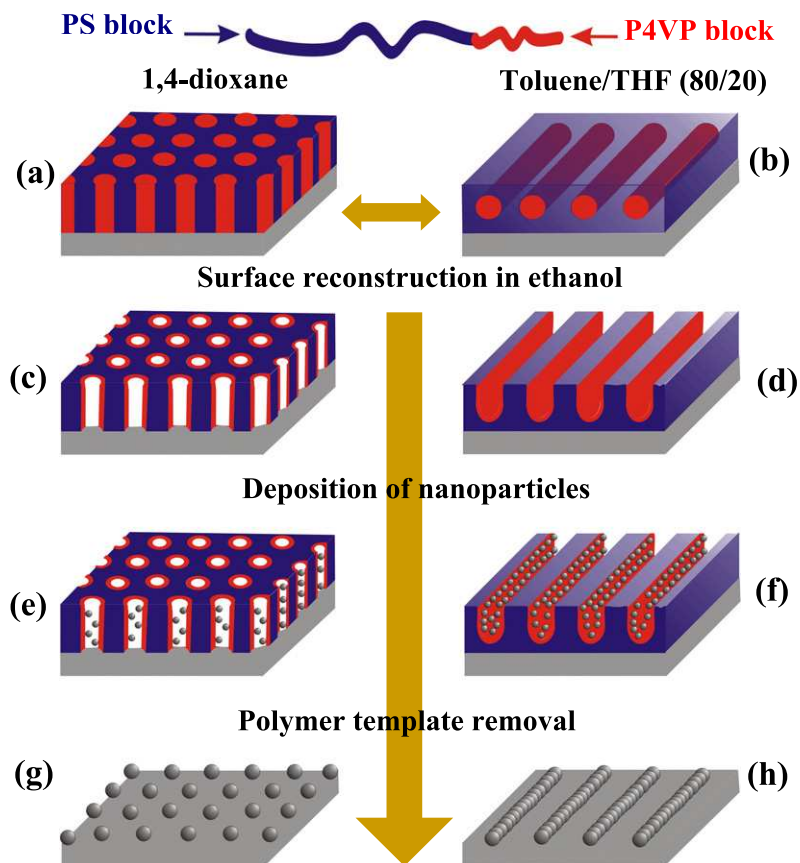


Figure 1. Schematic sketch of the fabrication process. (a), (b) Solvent annealed block copolymer thin films. The orientation of the cylinders is reversibly switchable in response to solvent vapors. (c), (d) Nanoporous films after surface reconstruction. (e), (f) Nanoparticles deposited onto templates. (g), (h) Highly ordered inorganic nanodots and nanowires remain on the silicon substrate after polymer removal.

assembly based on a PS-*b*-P4VP diblock copolymer with 2-(4'-hydroxybenzeneazo)benzoic acid. When the solvent annealed films were immersed into ethanol, a good solvent for P4VP and a non-solvent for PS, a surface reconstruction of the films was observed with a fine structure (figures 2(d) and (e)). Russell and co-workers have shown such a surface reconstruction process in PS-*b*-P4VP diblock copolymer thin films and demonstrated that the preferential solvation of P4VP blocks with ethanol does not alter the order or orientation of the microdomains [20c, 20d, 20e]. Surface reconstruction of a 1,4-dioxane annealed film ($C\perp$) keeps the well-developed microdomain structure, having perfect hexagonal order, as confirmed by fast Fourier transformation (inset), with an average center-to-center spacing of 26 ± 2 nm and pore diameter of 12 ± 1 nm (figure 2(d)). On the other hand, surface reconstruction of the films annealed in a mixture of toluene/THF (80/20) showed nanochannels parallel to the substrate ($C\parallel$) because of preferential solvation of the P4VP block (figure 2(e)) with a center-to-center spacing of $\sim 30 \pm 2$ nm.

Pre-synthesized palladium (Pd) nanoparticles were chosen to fill the block copolymer templates obtained above. One has to consider three important parameters in order to achieve selective deposition into the pores or channels of the templates. First, the size of the nanoparticles should be smaller than that of the nanopores. Transmission electron microscopy

(TEM) showed that nanoparticles had an average core diameter of 4 ± 1 nm (see supporting information, available at stacks.iop.org/Nano/20/415302) which is small enough to penetrate into nanopores of 12 ± 1 nm in diameter. Second, there should be a chemical interaction of the nanoparticles or their stabilizer with one of the copolymer blocks used. In our case the affinity can be either due to the citrate molecules stabilizing the nanoparticles in aqueous solution, which can be coordinated by the P4VP or it can be due to direct interactions of the palladium surface and the P4VP. Third, the dispersion media for nanoparticles is crucial since the block copolymer templates are in direct contact with the solution during the deposition process for longer times. The solvent chosen here must wet the inner pores of the template, but not swell or distort the template. Hence, the choice of solvent must be done carefully, in order to avoid the destruction of the template structure. In this study, an aqueous medium is the best choice to disperse the nanoparticles, since the nanopores of the template here were lined up with hydrophilic P4VP chains, which were surrounded by a hydrophobic PS matrix. Hence, the aqueous solution could selectively wet the cylindrical pores with the P4VP brushes, without disturbing the surrounding PS matrix.

The templates shown in figures 2(d) and (e) were immersed in an aqueous solution of Pd nanoparticles for 1 h at ambient temperature. After removal, the templates were repeatedly washed with deionized water in order to ensure

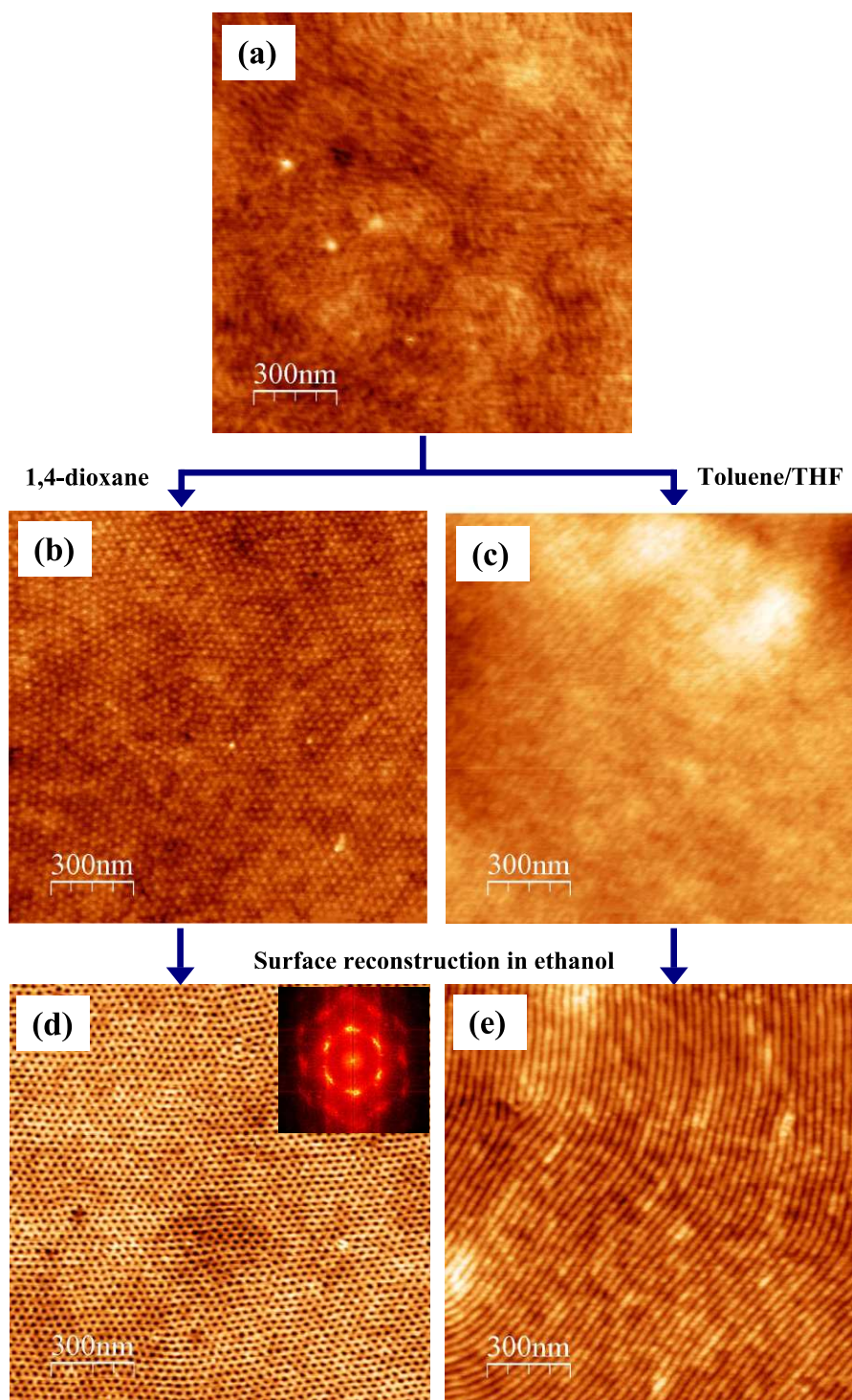


Figure 2. SFM height images of (a) a PS-*b*-P4VP film as dip-coated from the chloroform solution, (b) perpendicular oriented cylinders after annealing in 1,4-dioxane, (c) parallel oriented cylinders after annealing in toluene/THF (80/20) solvent mixture, (d) the 1,4-dioxane annealed film after surface reconstruction, and (e) the toluene/THF annealed film after surface reconstruction. The inset of (d) shows a fast Fourier transform image to show the long-range order.

the complete removal of the non-adsorbed or weakly adsorbed Pd nanoparticles. Figures 3(a) and (b) illustrate SFM height images of C_{\perp} and C_{\parallel} templates after the deposition of Pd nanoparticles. The SFM images show that the original structure was retained without any significant change except for a very few nanoparticles on the surface. The fast Fourier

transformation pattern shows that the lateral order was also retained perfectly after the nanoparticle deposition. Upon removal of the polymer template, highly ordered palladium dots and wires were obtained on the surface of silicon substrate, as shown in figures 3(c) and (d), exactly mirroring the pattern of the parent block copolymer template. Here,

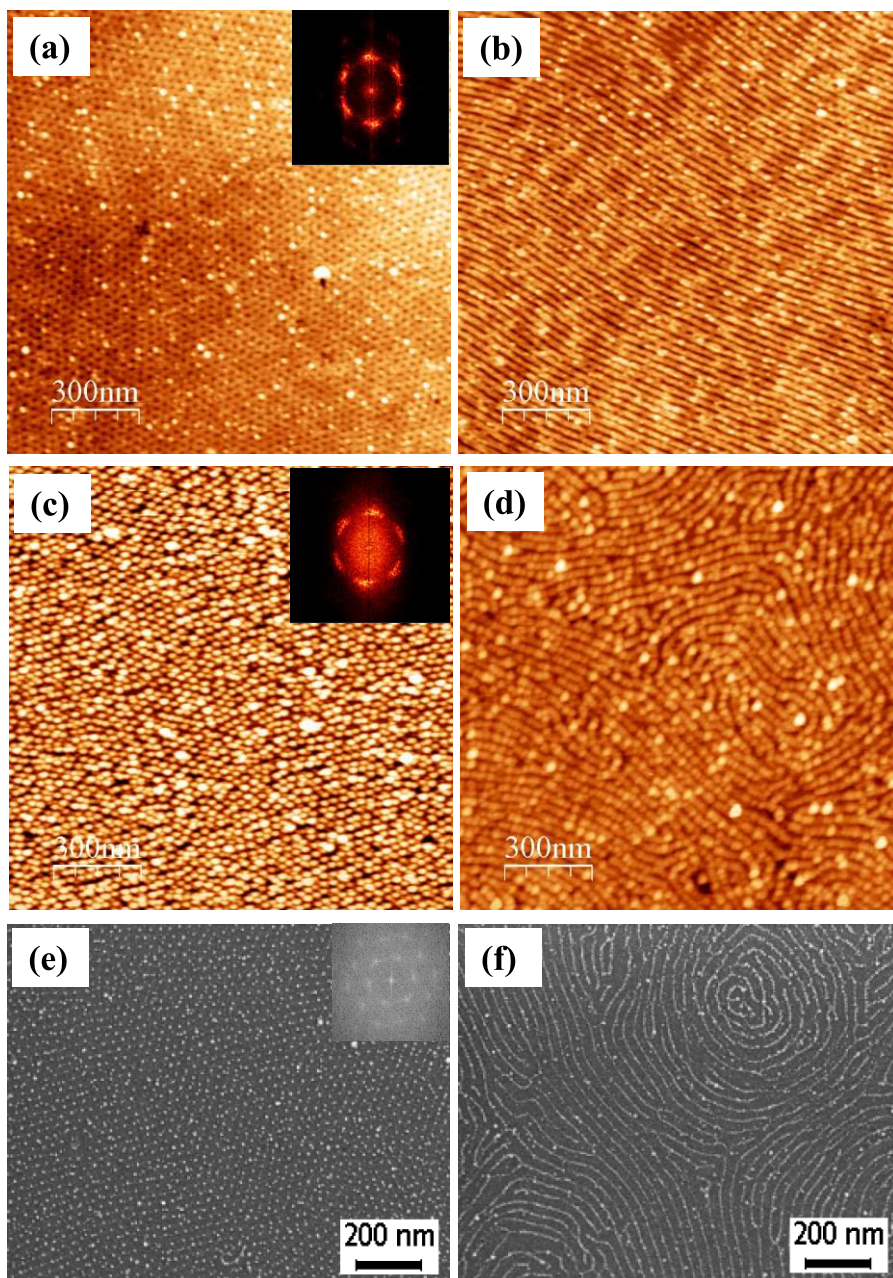


Figure 3. SFM height images of ((a), (b)) C_{\perp} and C_{\parallel} oriented cylindrical templates after the deposition of Pd nanoparticles, and ((c), (d)) Pd nanodots and nanowires obtained after the polymer removal. (e), (f) HRSEM images of Pd nanodots and nanowires after polymer removal.

the polymer films were removed by pyrolysis at 450°C in air. The polymer template was cross-linked under UV-irradiation to avoid segmental mobility of the polymer chains during pyrolysis (see supporting information, available at stacks.iop.org/Nano/20/415302). In case of Pd nanodots, the hexagonal packing was still maintained after polymer removal, which was again confirmed by the fast Fourier pattern (inset of figure 3(c)). In addition, the average center-to-center spacing of 26 ± 2 nm was also maintained. On the other hand, Pd nanowires also maintained the average center-to-center spacing of 30 ± 2 nm, similar to the parent block copolymer template. In both cases, the SFM section profile showed that the height of the nanodots or wires was almost similar to the mean diameter

of the nanoparticles (4 ± 1 nm). High-resolution scanning electron microscope (HRSEM) images further confirmed the formation of highly ordered dots and wires on the silicon substrate as shown in figures 3(e) and (f). The HRSEM images are almost similar to the SFM images, albeit there is a difference in the sizes of the nanodots/wires. The breadths of the nanodots and nanowires measured from HRSEM are almost same (12 ± 1 nm), and match the pore diameter of the parent template. It is important to note that the breadth of nanodots and wires appear much larger in the SFM image than the true values. This discrepancy can be attributed to the AFM tip surface convolution effects [44]. Another noteworthy result from the HRSEM observations is the formation of a

single nanodot or continuous wire-like structure from the agglomeration or fusion of nanoparticles within the pores or channels of the template after the polymer removal. It was due to the fact that, during pyrolysis, the nanoparticles within a single pore or channel were agglomerated or fused together to form a dot or wire as seen in HRSEM images. The Pd dots and wires obtained by this process have long-range lateral order with a uniform size over a wide area. We also used cylindrical templates prepared by supramolecular assembly (SMA) for the fabrication of nanodots and wires. In this different approach for the preparation of nanodots and wires we found that the nanostructures obtained are not as uniform as those reported here [45]. The formation of Pd nanostructures was further confirmed by x-ray photoelectron spectroscopy (XPS). The appearance of Pd(3d) signals at the characteristic binding energies of 335.1 and 340.3 eV indicates the presence of metallic Pd after template removal (see supporting information, available at stacks.iop.org/Nano/20/415302) [46]. It is worth mentioning here that Möller and co-workers fabricated metallic nanodots using PS-*b*-P2VP micelles by two different approaches [30–35]. In one approach, a metallic precursor or nanoparticle was embedded in the center of the diblock copolymer micelles before depositing it on the substrate. In another approach, PS-*b*-P2VP micelles were used as the nanocompartments to load the defined amount of a metal precursor. Subsequent hydrogen, oxygen or argon gas plasma treatment causes deposition of metal nanoparticles on the substrate. Their fabrication approaches are very different from the present work and also limited to the metallic nanodots.

It is necessary to understand the mechanism of nanoparticle penetration into the cylindrical pores or channels of the PS-*b*-P4VP templates. In these templates, the pore or channel walls are formed by the reactive P4VP chains. Hence, two possible driving forces can help fill the nanoparticles inside the pores or channels. The first one is the capillary force which allows the nanoparticle solution to enter inside the pores. Russell and co-workers used such capillary forces to fill nanoparticles into PS based porous templates [21]. They showed that the interaction of the solvent with the template is important for filling the pores as it determines the direction of the capillary force. As mentioned above, the aqueous solution used in our case for the dispersion of Pd nanoparticles can wet the pores effectively and uniformly because of the hydrophilic P4VP chains at the walls of nanopores. After loading the porous templates with nanoparticles by capillary forces, the templates were repeatedly washed with deionized water to remove the physically adsorbed nanoparticles. However, it has been found that the nanoparticles remained inside the pores or channels even after repeated washing. This means the nanoparticles were not simply physically adsorbed in the cavities of the templates. The capillary forces only help the nanoparticles to penetrate inside the pores, whereas the chemical interaction between P4VP chains and Pd nanoparticles is the key to holding the nanoparticles tightly inside the pores or channels.

In order to further confirm the role of interaction between P4VP chains and Pd nanoparticles, two simple experiments were performed. In one, UV cross-linked $C\perp$ and $C\parallel$

templates were utilized for the deposition of Pd nanoparticles in the same way as mentioned above. It was found that the filling of nanoparticles was not that uniform, compared to the uncross-linked templates, within a timeframe of 10 min immersion (see supporting information, available at stacks.iop.org/Nano/20/415302). This difference in deposition may be attributed to two basic reasons. The first reason may be the poor wetting of the cross-linked P4VP brushes which are at the walls of the nanopores. The second reason may be the poor interaction of cross-linked P4VP chains with Pd nanoparticles. In another experiment a thin film with $C\parallel$ oriented cylinders was directly used for the deposition process without reconstructing the surface, i.e. treating with ethanol. As shown in figure 2(c), the SFM image of the thin film with $C\parallel$ orientation is flat and more or less featureless, because the P4VP cylinders are buried within a uniform layer of PS. These films were used for the deposition process of Pd nanoparticles. Without surface reconstruction, no deposition of Pd was observed within a timeframe of 10 min, although prolonged immersion for 12 h resulted in some patches of nanoparticles on the surface (see supporting information, available at stacks.iop.org/Nano/20/415302). The hydrophobic PS, which is on the surface of the thin film, acts as a barrier between the P4VP chains and the aqueous solution of Pd nanoparticles. Hence, there is no efficient contact between P4VP chains and Pd nanoparticles to form nanostructures as observed above. In order to permit these P4VP chains in direct contact with Pd nanoparticles, surface reconstruction of the film is a prerequisite. In addition, these results also proved that the Pd nanoparticles were selectively coordinated only with P4VP domains and not with PS domains. We also used homopolymer films deposited on silicon wafers and treated them with a nanoparticle solution in the same way as for the block copolymer film. It was observed that Pd nanoparticles were immobilized on the flat P4VP surface and could not be removed even after rinsing with deionized water. It is noted that Pd nanoparticles were not observed on the PS homopolymer surface after a similar treatment which explains the selective decoration of nanoparticles in the pores.

We also extended this fabrication approach to other morphologies by choosing PS-*b*-P4VP samples having different molecular weights and volume fractions of their components. PS-*b*-P4VP copolymer (molecular weight of 39.0 kg mol^{-1} ($M_n^{\text{PS}} = 20.0 \text{ kg mol}^{-1}$; $M_n^{\text{P4VP}} = 19.0 \text{ kg mol}^{-1}$) and a polydispersity of 1.09) was dissolved in toluene/THF (80/20 v/v) solvent mixture at 70°C for 2 h to yield a 1 wt% polymer solution. Figure 4 shows the SFM height images of these samples after solvent vapor annealing in toluene/THF (80/20 v/v) mixture and 1,4-dioxane. The SFM images of a dip-coated sample (not shown here) and toluene/THF (80/20 v/v) vapor annealed samples showed dimple-type structures (dried micelles) (figure 4(a)). The formation of micelles was attributed to the selectivity of the solvent to one of the blocks. The toluene/THF (80/20 v/v) mixture chosen in this experiment selectively dissolves the PS and drives aggregation of the copolymer molecules to form micelles with an insoluble (P4VP) core and a soluble (PS) corona. The dimple-type of structure in solid films is far

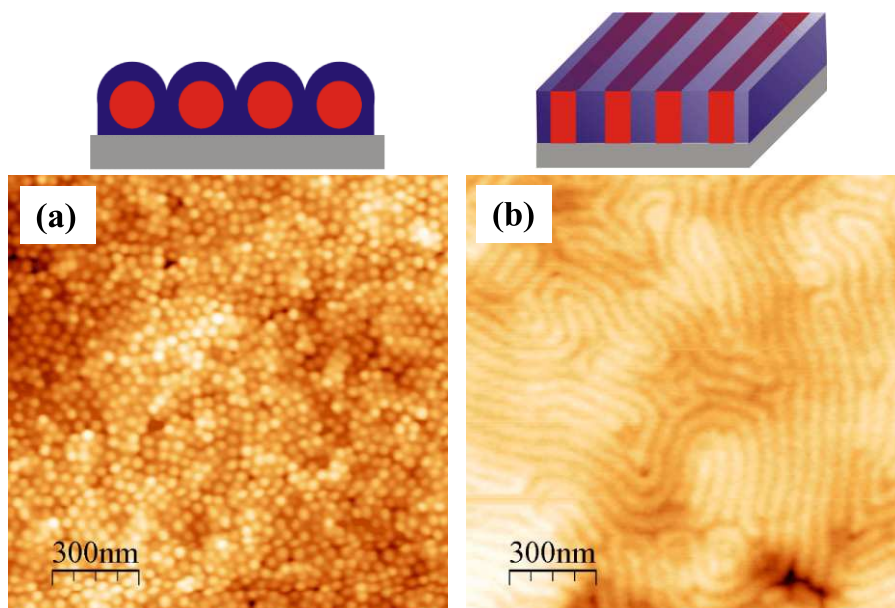


Figure 4. Schematic diagrams (top) and SFM height images (bottom) of (a) a dried PS-*b*-P4VP micelle film from toluene/THF (80/20) solution, and (b) lamellae after annealing in 1,4-dioxane.

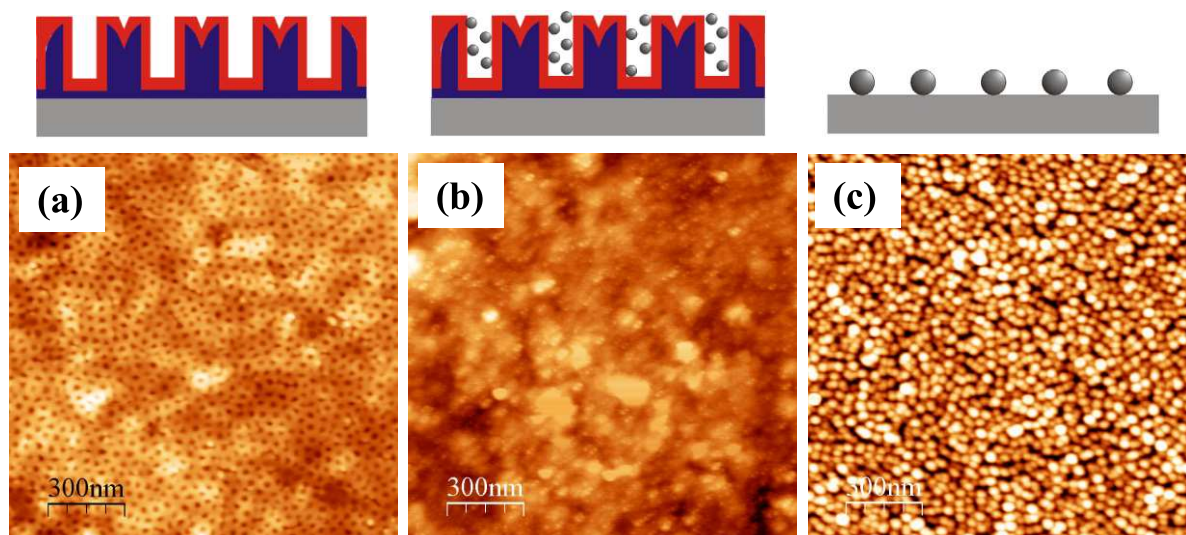


Figure 5. Schematic diagrams (top) and SFM height images (bottom) of surface-reconstructed dried micelles before (a) and after (b) the deposition of Pd nanoparticles, and (c) Pd nanodots obtained after polymer template removal.

from equilibrium and could be considered as a kinetically frozen structure due to rapid solvent evaporation. These structures are not retained upon annealing above the glass transition temperature or in saturated vapors of other non-selective solvents. Further annealing of this dimple-type structure in saturated vapors of 1,4-dioxane causes the thin film to reorganize into a highly oriented lamellar structure normal to the substrate (figure 4(b)). Recently, Park *et al* [47] also reported such a dimple-type structure in PS-*b*-P4VP thin films using toluene/THF mixture as a solvent. In this case, we used ethanol vapors to reconstruct the surface instead of immersing the sample directly in ethanol. It was found that the direct immersion of micelles or lamellae into ethanol ruined the

structure. Figures 5(a) and 6(a) show the SFM height images of these samples after surface reconstruction in ethanol. We clearly observed an inverted pattern of micelles resulting in an array of nanoholes with the same periodicity (40 ± 2 nm) as the micellar arrays (figure 4(a)). Such micellar inversion without a change of micellar packing was also observed by other authors [48, 49]. On the other hand, a huge contrast difference was observed in the SFM image of the lamellar structure before and after the surface reconstruction (figures 4(b) and 6(a)) suggesting that the P4VP chains are partially exposed to the surface. Also, we observed that the lamellar spacing did not change (51 ± 2 nm) during the surface reconstruction.

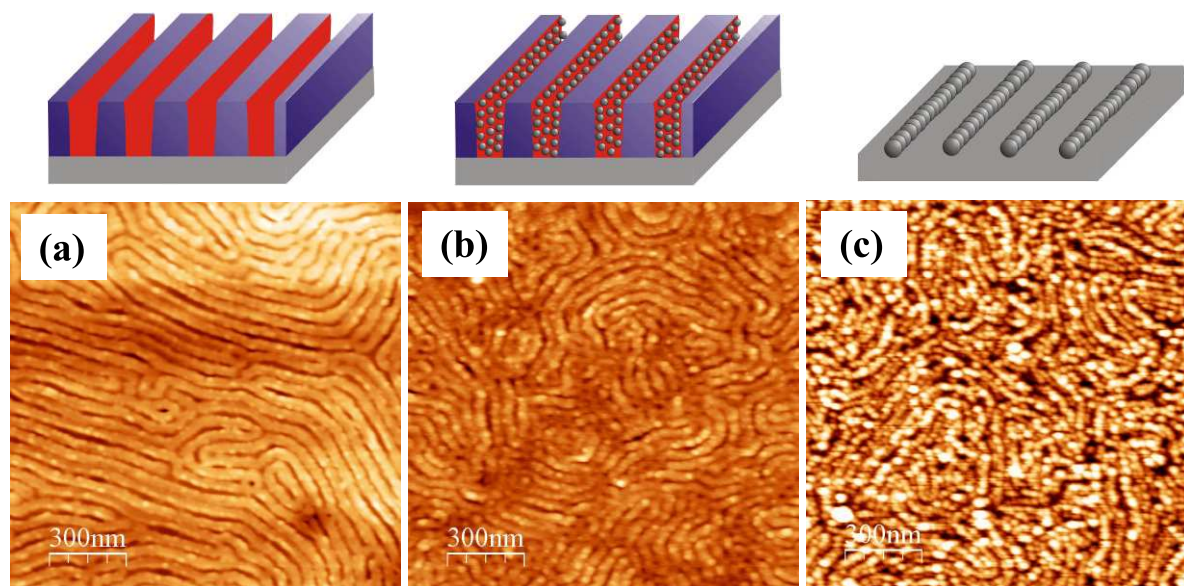


Figure 6. Schematic diagrams (top) and SFM height images (bottom) of surface-reconstructed lamellae before (a) and after (b) the deposition of Pd nanoparticles, and (c) Pd nanowires obtained after polymer template removal.

The templates shown in figures 5(a) and 6(a) were used for the deposition of Pd nanoparticles, and the deposition procedure is the same as discussed above. Figures 5(b) and (c) illustrate SFM height images of Pd deposited micellar templates before and after removal of the polymer. The average center-to-center spacing of Pd nanodots was 40 ± 2 nm, which is almost similar to the center-to-center spacing of the starting micelles. Figures 6(b) and (c) illustrate SFM images of Pd deposited onto a lamellar template before and after removal of the polymer. The nanowires produced in the case of lamellar structures were found to be disordered in comparison to the wires produced from $C\parallel$ cylindrical templates. In this way, we demonstrated the general applicability of our technique to other morphologies.

Acknowledgments

EBG is grateful to the Alexander von Humboldt foundation for a research fellowship. The authors thank Dr Petr Formanek for SEM, Dr Paul Simon for TEM and Dr Frank Simon for XPS measurements. This research was supported by the priority program of Deutsche Forschungsgemeinschaft (SPP1165, Project No. STA324/31) as well as the project STABILIGHT and the NoE PHOREMOST within framework program 6 of the European Union.

References

- [1] Gates B D, Xu Q, Stewart M, Ryan D, Willson C G and Whitesides G M 2005 *Chem. Rev.* **105** 1171
- [2] Bratton D, Yang D, Dai J and Ober C K 2006 *Polym. Adv. Technol.* **17** 94
- [3] Gates B D, Xu Q, Love J C, Wolfe D B, Willson C G and Whitesides G M 2004 *Annu. Rev. Mater. Res.* **34** 339
- [4] Xia Y, Rogers J A, Paul K E and Whitesides G M 1999 *Chem. Rev.* **99** 1823
- [5] Mansky P, Harrison C K, Chaikin P M, Register R A and Yao N 1996 *Appl. Phys. Lett.* **68** 2586
- [6] Melosh N A, Davidson P and Chmelka B F 2000 *J. Am. Chem. Soc.* **122** 823
- [7] Li R R, Dapkus P D, Thompson M E, Jeong W G, Harrison C, Chaikin P M, Register R A and Adamson D H 2000 *Appl. Phys. Lett.* **76** 1689
- [8] Park M, Harrison C, Chaikin P M, Register R A and Adamson D H 1997 *Science* **276** 1401
- [9] Lopes W A and Jaeger H M 2001 *Nature* **414** 735
- [10] Thurn-Albrecht T, Schotter J, Kastle G A, Emley N, Shibauchi T, Krusin-Elbaum L, Guarini K, Black C T, Tuominen M T and Russell T P 2000 *Science* **290** 2126
- [11] Cheng J Y, Ross C A, Chan V Z H, Thomas E L, Lammertink R G H and Vancso G J 2001 *Adv. Mater.* **13** 1174
- [12] Park C, Yoon J and Thomas E L 2003 *Polymer* **44** 7779
- [13] Bates F S and Fredrickson G H 1999 *Phys. Today* **52** 32
- [14] Krausch G and Magerle R 2002 *Adv. Mater.* **14** 1579
- [15] Ruzette A V and Leibler L 2005 *Nat. Mater.* **4** 19
- [16] Segalman R A R 2005 *Mater. Sci. Eng.* **48** 191
- [17] Hawker C J and Russell T P 2005 *MRS Bull.* **30** 952
- [18] Morkved T L, Lu M, Urbas A M, Ehrichs E E, Jaeger H M, Mansky P and Russell T P 1996 *Science* **16** 931
- [19] Park C, Yoon J and Thomas E L 2003 *Polymer* **44** 6725
- [20] Kim J K, Lee J I and Lee D H 2008 *Macromol. Res.* **16** 267
- [21] Kim G and Libera M 1998 *Macromolecules* **30** 2569
- [22] Jeong U, Ryu D Y, Kim J K, Kim D H, Wu X and Russell T P 2003 *Macromolecules* **36** 10126
- [23] Jeong U, Ryu D Y, Kho D H, Kim J K, Goldbach J T, Kim D H and Russell T P 2004 *Adv. Mater.* **16** 533
- [24] Darling S B 2007 *Prog. Polym. Sci.* **32** 1152
- [25] Crossland E J W, Ludwigs S, Hillmyer M A and Steiner U 2007 *Soft Matter* **3** 94
- [26] Xu T, Stevens J, Villa J, Goldbach J T, Guarini K W, Black C T, Hawker C J and Russell T P 2003 *Adv. Funct. Mater.* **13** 698
- [27] Xu T, Stevens J, Villa J, Goldbach J T, Guarini K W, Black C T, Hawker C J and Russell T P 2003 *Adv. Funct. Mater.* **13** 698
- [28] Xu T *et al* 2004 *Macromolecules* **37** 2972
- [29] Park S, Kim B, Wang J Y and Russell T P 2008 *Adv. Mater.* **20** 681

- [20d] Park S, Wang J Y, Kim B, Xu J and Russell T P 2008 *ACS Nano* **2** 766
- [20e] Park S, Wang J Y, Kim B and Russell T P 2008 *Nano Lett.* **8** 1667
- [21] Misner M J, Skaff H, Emrick T and Russell T P 2003 *Adv. Mater.* **15** 221
- [22] Zhang Q, Xu T, Butterfield D, Misner M J, Ryu D Y, Emrick T and Russell T P 2005 *Nano Lett.* **5** 357
- [23] Lo K-H, Tseng W H and Ho R-M 2007 *Macromolecules* **40** 2621
- [24] Ansari I A and Hamley I W 2003 *J. Mater. Chem.* **13** 2412
- [25] Lin Y *et al* 2005 *Nature* **434** 55
- [26] Chiu J J, Kim B J, Kramer E J and Pine D J 2005 *J. Am. Chem. Soc.* **127** 5036
- [27] Minelli C, Hinderling C, Heinzelmann H, Pugin R and Liley M 2005 *Langmuir* **21** 7080
- [28] Thompson R B, Ginzburg V V, Matsen M W and Balazs A C 2001 *Science* **292** 2469
- [29] Thompson R B, Ginzburg V V, Matsen M W and Balazs A C 2002 *Macromolecules* **35** 1060
- [30] Spatz J P, Herzog T, Mößmer S, Ziemann P and Möller M 1999 *Adv. Mater.* **11** 149
- [31] Spatz J P, Mößmer S, Hartmann C, Möller M, Herzog T, Krieger M, Boyen H-G, Ziemann P and Kabius B 2000 *Langmuir* **16** 407
- [32] Spatz J P, Chan V Z H, Mößmer S, Kamm F, Plettl A, Ziemann P and Möller M 2002 *Adv. Mater.* **14** 1827
- [33] Spatz J P, Chan V Z-H, Mößmer S, Möller M, Kamm F-M, Plettl A and Ziemann P 2002 *Adv. Mater.* **14** 1027
- [34] Kästle G *et al* 2003 *Adv. Funct. Mater.* **13** 853
- [35] Glass R, Möller M and Spatz J P 2003 *Nanotechnology* **14** 1153
- [36] Chai J and Buriak J M 2008 *ACS Nano* **2** 489
- [37] Chai J, Wang D, Fan X and Buriak J M 2007 *Nat. Nanotech.* **2** 500
- [38] Haryono A and Binder W H 2006 *Small* **2** 600
- [39] Hamley I W 2003 *Angew. Chem. Int. Edn* **42** 1692
- [40] Kim B J, Chiu J J, Yi G, Pine D J and Kramer E J 2005 *Adv. Mater.* **17** 2618
- [41] Thurn-Albrecht T, Steiner R, DeRouchey J, Stafford C M, Huang E, Bal M, Tuominen M, Hawker C J and Russell T P 2000 *Adv. Mater.* **12** 787
- [42] Sidorenko A, Tokarev I, Minko S and Stamm M 2003 *J. Am. Chem. Soc.* **125** 12211
- [43] Tokarev I, Sidorenko A, Minko S and Stamm M 2004 *Polym. Mater. Sci. Eng.* **90** 292
- [44] Grabar K C, Brown K R, Keating C D, Stranick S J, Tang S L and Natan M J 1997 *Anal. Chem.* **69** 471
- [45] Nandan B, Gowd E B, Bigall N C, Eychmüller A, Formanek P, Simon P and Stamm M 2009 *Adv. Funct. Mater.* **19** 2805
- [46] Moulder J F, Stickle W F, Sobol P E and Bomben K D 1984 *Handbook of X-ray Photoelectron Spectroscopy* ed J Chastain (Eden Prairie, MN: Perkin-Elmer)
- [47] Park S, Wang J Y, Kim B, Chen W and Russell T P 2007 *Macromolecules* **40** 9059
- [48] Sohn B H, Yoo S I, Seo B W, Yun S H and Park S M 2001 *J. Am. Chem. Soc.* **123** 12734
- [49] Krishnamoorthy S, Pugin R, Brugger J, Heinzelmann H, Hoogerworf A C and Hinderling C 2006 *Langmuir* **22** 3450